



HAL
open science

Modulating the Physical and Electronic Properties over Positional Isomerism: The Dispirofluorene–Dihydroindacenodithiophene (DSF-IDT) Family

J.-D. Peltier, B. Heinrich, B. Donnio, O. Jeannin, J. Rault-Berthelot, Cyril Poriel

► To cite this version:

J.-D. Peltier, B. Heinrich, B. Donnio, O. Jeannin, J. Rault-Berthelot, et al.. Modulating the Physical and Electronic Properties over Positional Isomerism: The Dispirofluorene–Dihydroindacenodithiophene (DSF-IDT) Family. *Chemistry - A European Journal*, 2017, 23 (68), pp.17290-17303. 10.1002/chem.201703320 . hal-01671610

HAL Id: hal-01671610

<https://univ-rennes.hal.science/hal-01671610>

Submitted on 1 Feb 2018

HAL is a multi-disciplinary open access archive for the deposit and dissemination of scientific research documents, whether they are published or not. The documents may come from teaching and research institutions in France or abroad, or from public or private research centers.

L'archive ouverte pluridisciplinaire **HAL**, est destinée au dépôt et à la diffusion de documents scientifiques de niveau recherche, publiés ou non, émanant des établissements d'enseignement et de recherche français ou étrangers, des laboratoires publics ou privés.

Modulating the physical and electronic properties over positional isomerism: the Dispirofluorene-Dihydroindacenodithiophene (DSF-IDT) family.

Jean-David Peltier,^[a] Benoît Heinrich,^[b] Bertrand Donnio,^[b] Olivier Jeannin,^[a] Joëlle Rault-Berthelot,^{[a]*} Cyril Poriel^{[a]*}

^[a] UMR CNRS 6226-ISCR-Université de Rennes 1-35042 Rennes cedex-France

^[b] Institut de Physique et Chimie des Matériaux de Strasbourg, UMR 7504, CNRS-Université de Strasbourg, 23 rue du Loess, BP 43, 67034, Strasbourg Cédex 2 France

E-mail: cyril.poriel@univ-rennes1.fr, joelle.rault@univ-rennes1.fr, jean-david.peltier@univ-rennes1.fr, olivier.jeannin@univ-rennes1.fr, Benoit.Heinrich@ipcms.unistra.fr, bertrand.donnio@ipcms.unistra.fr

TOC

We report the first studies on the intrinsic properties of a *meta*-substituted dihydroindacenodithienyl fragment and more generally the strong impact of positional isomerism on dihydroindacenodithiophene derivatives. The influence of the *para* and *meta* linkages has notably been highlighted not only on the electronic properties in solution (electrochemical properties, anodic polymerization, HOMO/LUMO energy levels, optical transitions, fluorescence spectra...) but also on the physical properties in the solid state (molecular organization, crystallinity and phase transitions). The positional isomerism hence appears as a very efficient tool to drastically tune the properties of dihydroindacenodithiophene derivatives.

Keywords

DiSpiroFluorene-Indacenodithiophenes, spiro compounds, 3 π -2spiro architecture, isomerism, structure-activity relationships, electropolymerization

Abstract

We report the first studies on the intrinsic properties of a *meta*-substituted dihydroindacenodithienyl fragment and more generally the strong impact of positional isomerism on dihydroindacenodithiophene derivatives. The influence of the *para* and *meta* linkages has notably been highlighted not only on the electronic properties in solution (electrochemical properties, anodic polymerization, HOMO/LUMO energy levels, optical transitions, fluorescence spectra...) but also on the physical properties in the solid state (molecular organization, crystallinity and phase transitions). The positional isomerism hence appears as a very efficient tool to drastically tune the properties of dihydroindacenodithiophene derivatives.

Introduction

The modulation of the physico-chemical and photophysical properties of organic semiconductors (OSCs) to fit the necessary requirements needed for an electronic device, namely organic light-emitting diodes (OLED or PhOLED),^[1-8] organic-field-effect transistors (OFET),^[9-12] and organic photovoltaics (OPV),^[13-17] is the heart of organic electronics (OE) and has allowed its fantastic emergence. The dihydroindacenodithiophene (IDT) fragment is an important building unit, which gathers two thienyl cores to a central phenyl ring. IDT based OSCs have been used as small molecules,^[18-24] polymers or copolymers^[25-29] mainly for OPV applications.^[30] However, with a few exceptions,^[31-32] nearly all the IDT-based molecules described to date in the literature possess a central *para*-linked phenyl with the two sulfur atoms in an *anti*-configuration. In the last years, the positional isomerism has proved to be a very efficient tool to tune the properties of OSCs.^[33-49] Particularly, the '3 π -2spiro' molecular architectures, developed by ones of us a decade ago,^[49-55] (association of three π -systems via two spiro bridges, Figure 1) have shown how the positional isomerism can drastically modified the fluorescence and/or phosphorescence properties of an OSC leading to very efficient materials for blue emitting OLEDs and PhOLEDs. The efforts have nevertheless been mainly centered on the positional isomerism of the dihydroindenofluorene core (IF), which is a bridged terphenyl unit (Figure 1, Top).
^[33, 35, 39-40, 56-57]

Figure 1. Dihydroindacenodithienyl derivatives **meta-DSF-IDT** and **para-DSF-IDT** investigated in this work (bottom) and two dihydroindenofluorenyl analogues **[1,2-b]-DSF-IF** and **[2,1-b]-DSF-IF** (top).

In this context, we have recently been interested on the impact of positional isomerism of IDT fragments.^[32] Thus, an IDT isomer possessing a central *meta*-linked phenyl unit and the two sulfur atoms in a *syn* configuration has been designed. Efficient n-type OFETs have been obtained and the influence of the positional isomerism on the device performance has particularly been noted.^[32] Nevertheless, in these previous works, the bridges of the IDT fragments were substituted with the strong electron deficient dicyanovinylene functionalities, which drastically change the electronic properties of the IDT cores. In the present study, we wish to investigate the intrinsic properties of the *meta*-substituted IDT core, never reported to date, through a fine structure properties relationship study with its *para*-substituted isomer. For that purpose, two new molecules namely **para-DSF-IDT** and **meta-DSF-IDT** based on a '3 π -2spiro' architecture have been designed, synthesized and studied (see structures in Figure 1). They possess (i) two different central IDT cores with either a *para* or a *meta*-phenyl/thienyl linkage, (ii) two fluorenyl units spiro-linked to the IDT core and (iii) two hexyl chains on the IDT core for purpose of solubility. After synthetic details, their structural, photophysical and

physicochemical properties will be analyzed and compared (i) with each other from the standpoint of the influence of the linkage on the central IDT cores, and (ii) to structurally related DiSpiroFluorene-Indenofluorenes (DSF-IFs) possessing either a central *para*-substituted IF core (bridged *para*-terphenyl unit), namely dispiro[fluorene-9,11'-indeno[1,2-*b*]fluorene-12',9''-fluorene] **[1,2-*b*]-DSF-IF** or a central *meta*-substituted IF core (bridged *meta*-terphenyl unit), namely dispiro[fluorene-9,5'-indeno[2,1-*b*]fluorene-7',9''-fluorene] **[2,1-*b*]-DSF-IF** (Figure 1), in order to shed light on the influence of the bridged thienyl units.

[1-22, 25, 27-30, 32-42, 48-56, 58]

Results and discussion

Synthesis

Scheme 1. Retrosynthetic approaches to **DSF-IF** (top) and **DSF-IDT** (bottom)

The synthetic approaches to both **para-DSF-IDT** and **meta-DSF-IDT** isomers were inspired by the retrosynthetic analyses of the previously reported **[1,2-*b*]-DSF-IF** (*para* isomer) and **[2,1-*b*]-DSF-IF** (*meta* isomer) analogues (Scheme 1, Top).^[40, 42, 50, 52] Indeed, as **para-DSF-IDT** and **meta-DSF-IDT** can be considered as the fusion of two indacenothiophenyl units, they can be obtained along two main different routes (A and B).

In the case of DSF-IF derivatives, route A included a double lithium-halogen exchange reaction (Scheme 1, Top, Route A) and either involved a *meta* or *para* diiodoterphenyl as the key starting material.^[50-51] Despite the efficiency of this route, a similar synthetic approach might not be used to prepare **para-DSF-IDT** and **meta-DSF-IDT** as the key diiodinated intermediates di(thiophen-2-yl)benzene appeared to be complicated to synthesize (Scheme 1, Bottom, Route A). Moreover, it has been shown in the last years that such synthetic approach is not regioselective and can lead to positional isomers of DSF-IFs with either a *syn* or an *anti* geometry.^[33, 39, 49, 57] Thus, another synthetic strategy, this time regioselective, has been envisaged for both **[1,2-*b*]-DSF-IF**⁴⁶ and **[2,1-*b*]-DSF-IF** (Scheme 1, Top, Route B) and will be used herein for the thienyl analogues (Scheme 1, Bottom, Route B). The key feature in this regioselective approach is to build up the IDT core (or IF core for DSF-IFs) prior to the final cyclization step in order to avoid isomers formation. In this approach, the corresponding diketones **para-IDT(=O)₂** and **meta-IDT(=O)₂** are the key intermediates and their syntheses have previously been reported in the literature from diethyl 4,6-dibromoisophthalate^[32] and diethyl 2,5-dibromoterephthalate respectively.^[23, 32]

Scheme 2. Synthesis of **para-DSF-IDT** and **meta-DSF-IDT**

Thus, as shown in Scheme 2, the lithium-iodine exchange of 2-iodobiphenyl with *n*-butyllithium at low temperature followed by the quenching with either **para-IDT(=O)₂** or **meta-IDT(=O)₂** afforded the corresponding dihydroindacenodithiophenols which were not purified at this stage and were immediately involved in the intramolecular cyclization reaction in acidic media (CH₂Cl₂/BF₃- etherate). **Para-DSF-IDT** and **meta-DSF-IDT** were respectively obtained with a yield of 68% and 65% (after recrystallization). In contrast to the dicyanovinylene analogues previously reported,^[32] both isomers exhibit good solubility in common organic solvents such as CHCl₃, CH₂Cl₂, THF and DMF.

It should be noted that the synthesis of non-spiro configured *para*-IDT and *meta*-IDT derivatives reported in literature by Wong and coworkers^[31] used a similar approach starting from diethyl 4,6-dibromoisophthalate and diethyl 2,5-dibromoterephthalate respectively, however, the characterization of the diketones was not described surely due to their very low solubility in absence of hexyl units on the IDT cores.

Figure 2. A portion of ¹H NMR spectra (CD₂Cl₂) of left : **[2,1-*b*]-DSF-IF**^[39] (top) and **[1,2-*b*]-DSF-IF**^[48] (bottom) and right : **para-DSF-IDT** (top) and **meta-DSF-IDT** (bottom).

At this stage, the fine comparative analyses of the ¹H NMR spectra of **para-DSF-IDT** with its **[1,2-*b*]-DSF-IF** analogue^[48] and **meta-DSF-IDT** with its **[2,1-*b*]-DSF-IF** analogue^[39] can provide interesting informations on the influence of the incorporation of the thienyl rings on the chemical shift of the hydrogen atoms (Figure 2). The complete assignments have been performed by 2D NMR spectroscopy experiments: HMBC (Heteronuclear Multiple Bond Correlation), HSQC (Heteronuclear Single Quantum Coherence) and ¹H/¹H COSY (Correlation Spectroscopy), see Figure S40-S51 in SI.

First, one can note that the hydrogen atom borne by the thienyl ring, H5, in **para-DSF-IDT** and **meta-DSF-IDT** is recorded at a very similar chemical shift (δ = 6.09 vs 6.02 ppm), clearly highlighting that the nature of the linkage (*para* vs *meta*) has no/little influence on the chemical shifts of this hydrogen atom. However, the linkages have a clear effect on the chemical shift of the hydrogen atoms (H9 and H10) of the central phenyl ring and deserve a particular attention. Indeed, for the **para-DSF-IDT** isomer, the two hydrogen atoms borne by this central phenyl ring, H9, are detected at 6.66 ppm, being strongly shielded compared to those of the **[1,2-*b*]-DSF-IF** analogue (δ = 7.18 ppm), which also possesses *para* linkages.^[48] This strong shielding effect is assigned to the substitution of the phenyl ring in **[1,2-*b*]-DSF-IF** by the thienyl ring in **para-DSF-IDT** and the resulting enhancement of the electron rich character.

As the symmetry of the **meta-DSF-IDT** isomer is different, two resonances are detected for the hydrogen atoms of the central phenyl ring, (δ_{H9} = 7.59 ppm, δ_{H10} = 5.86 ppm,). First, one can note that H10 appears at a very low chemical shift of 5.86 ppm as it is influenced by two spiro-linked fluorene units whereas in the **para-DSF-IDT** analogue, only one fluorene directly influences

central hydrogen atoms. It has been indeed previously evidenced that spiro-linked fluorenes leads to a significant shielding effect.^[48] This effect is also found herein for **meta-DSF-IDT**. In addition, the two cofacial fluorene fragments and their associated shielding cones are also surely responsible of the very low chemical shift of H10. Indeed, trans-annular π - π interactions are usually accompanied by high field shifts in ¹H NMR spectra.^[48-49, 59-63] In **[2,1-b]-DSF-IF**, H10 is also found at a high field, 6.11 ppm,^[39] but remains nevertheless less shielded than in **meta-DSF-IDT**. Thus in **meta-DSF-IDT**, the presence of (i) thienyl rings and (ii) cofacial fluorenes both contribute to the strong shielding of the central proton H10 below 6 ppm. It should also be mentioned that for a structurally related *meta*-IDT core substituted on the bridges by two tolyl units,^[31] there is no trace of such highly shielded hydrogen atom (the corresponding H9 and H10 protons are reported at 7.52 and 7.38 ppm with however no precise assignment stated). This clearly confirms the key role played by the cofacial fluorene herein on the shielding of the central hydrogen atom H10.

On the other hand, the H9 resonance in **meta-DSF-IDT** is detected at 7.59 ppm, being strongly deshielded compare to that of H10

(5.86 ppm) and translating the very different chemical environment of these hydrogen atoms. This is caused by the presence of the two thienyl cores in α position of H9. More importantly, in **[2,1-b]-DSF-IF**, the same hydrogen atom H9 is found at 8.38 ppm,^[39] significantly deshielded by 0.79 ppm compared to that of **meta-DSF-IDT**. Thus, the presence of the bridged thiophenes and their electron rich character in **meta-DSF-IDT** and **para-DSF-IDT** leads to a strong shielding effect of the central hydrogen atoms (0.52 ppm for the *para*-substituted and 0.79 ppm for the *meta* substituted) compared to their DSF-IF analogues with their phenyl units.

Physicochemical properties of DSF-IDT derivatives

Structural properties: Single crystals of **para-DSF-IDT** and **meta-DSF-IDT** were obtained from a chloroform/methanol mixture in crystals of sufficient quality to elucidate their molecular structures and packing characteristics. The structure of both molecules is presented figure 3 (see Figures S4- S9 and Figures S13-S22 in supplementary data for a more detailed description of each structure).

Figure 3. Molecular structures from X-ray crystallography of **para-DSF-IDT** (Top) and **meta-DSF-IDT** (Bottom). The hydrogen atoms have been omitted for clarity. In b) and c), the hexyl chains have been reduced to methyl groups for purpose of clarity.

Para-DSF-IDT crystallizes in the $P4_2/n$ space group. The central *para*-substituted IDT core (rings 1 to 5) has a length of 10.55 Å similar to that reported by Wong^[31] for a non-spiro analogue (10.46 Å) (Figure 3, Top-middle). The two spiro angles (angle between the mean planes of ring 2 and that of ring 10 and angle between the mean planes of ring 7 and ring 4) are recorded at ca 89.5°, showing the orthogonality between the two fluorene units and the central IDT core as generally observed for compounds possessing a 3 π -2spiro architecture.^[33, 35-36, 39-40, 50] Due to the *para* linkages, the central *para*-substituted IDT core is almost flat with a small dihedral angle of 3.39° between the two mean planes of the external thienyl cores 1 and 5 (Figure 3, Top-right). In addition, we measured a distance of 0.28 Å between the two mean planes of the thienyl units which are parallel.

Drastically different structural properties are observed for **meta-DSF-IDT** isomer which crystallizes in the $P4/ncc$ space group, with nevertheless some disorder on the fluorene formed by rings 6-8 (see in blue a second possible position of the fluorene in Figure 3, Bottom-left). The central *meta*-IDT core of **meta-DSF-IDT** (rings 1-5) has a length of 9.92 Å being shorter than that of **para-DSF-IDT** (10.55 Å) due to the different linkages (*para* vs *meta*) of the constituting phenyl rings (Figure 3, Bottom-middle). This contraction of the *meta*-substituted IDT core is caused by its "crescent moon" shape. The *meta* linkages of **meta-DSF-IDT** also lead to a strong deformation of its central core, with a dihedral angle of 14.36° detected between the two mean planes of the external thienyl cores 1 and 5 (Figure 3, Bottom-right). This behavior is not observed for the *para*-substituted IDT core of **para-DSF-IDT**, which is almost flat (deformation of 3.39°, see above) and hence confirms the key role played by the linkages on the molecular distortion. The spiro- angles are also very close to 90° (89.9 between rings 4 and 10 and 89.01° between rings 2 and 7, or 87.83° for the fluorene in blue), clearly showing the orthogonality between the two fluorene units and the central IDT core. In addition, the two fluorenyl units do not display a perfect eclipsed conformation and the distance between the two spiro carbons is measured at ca 5.24 Å, indicating that the two face-to-face fluorene units are too far one from another to allow intramolecular π -stacking interactions.*

Finally, compared to the *para* and *meta* bridged terphenyl cores, namely dihydroindeno[1,2-*b*]fluorene^[51] and dihydroindeno[2,1-*b*]fluorene^[39], previously reported in literature for structurally related analogues **[1,2-b]-DSF-IF** and **[2,1-b]-DSF-IF** respectively, one may note that both *para*- and *meta*-substituted IDT cores are shorter (decrease from 11.1 Å to 10.55 Å for the *para* cores and from 10.6 Å to 9.92 Å for the *meta* ones). The shortening of the central core is obviously due to the substitution of the two external phenyl units by two smaller thienyl units but not only. Indeed, the shortening is more important in the *meta* series (0.68 Å) than in the *para* series (0.55 Å). The second origin of the shortening may come from the bending of the central core, which is more important for the *meta*-substituted IDT core than for the IF cores (the dihedral angle between the mean planes of the external thienyl or phenyl units is as high as 14.36° for **meta-DSF-IDT** and is only 2.25° for **[2,1-b]-DSF-IF**). Thus, the deformations appear to be different as a function of both the linkages (*meta* vs *para*) and the constituted rings (thienyl vs phenyl).

Self-organization properties. The different molecular shapes of both isomers lead to different crystalline self-assemblies. The central phenyl of the IDT backbones of the **para-DSF-IDT** compound occupy the nodes of a centered square lattice ($a = 21.4919$ Å, $Z_{2D} = 2$) and arrange in rows perpendicular along to the square diagonal, which alternate with rows formed by the intercalated alkyl chains (Figure 4 Top and additional Figures S10-S12 in supplementary data). In such an arrangement, the IDT units and the alkyl chains are confined in a thin corrugated sheet, whilst the fluorenyl units point out of the sheet surface, and intercalate with the fluorenyl units of the next molecular layer. The IDT cycles of the top molecular layer are placed in the middle of four neighboring IDT cycles of

* For structural features related to other dispirofluorene-indenofluorene with interacting face-to-face fluorene units, see references^{34,50,56}

the bottom layer, with the rows directed along the other square diagonal. The periodicity corresponds thus of two staggered layers and results in the $P4_2/n$ cell involving $Z = 4$ molecules ($a = b = 21.4919 \text{ \AA}$, $c = 8.4063 \text{ \AA}$).

Figure 4. Crystal packing in the $a \times b$ planes obtained from X-ray crystallography of **para-DSF-IDT** (top) and **meta-DSF-IDT** (bottom). Left: top monolayer, middle: bottom layer and right all the layers. The hydrogen atoms have been omitted for clarity, in blue the IDT cores, in red the fluorenes and in green the alkyl chains.

The **meta-DSF-IDT** isomer forms on the contrary a lamellar crystalline structure resulting by an alternated sequence of discrete molecular bilayers (lamellar periodicity: $d = 11.13 \text{ \AA}$) (see Figure 4, bottom and additional Figures S23-S29 in supplementary data) The median strata of the bilayers are formed by head-to-tail arranged fluorenyls, while the **IDT** units and the alkyl chains are rejected aside toward the bilayer borders. Within bilayers, the **DSF-IDT** moieties self-associate in aggregates of 4 molecules, which in turn arrange in a centered square lattice ($a = 27.4775 \text{ \AA}$, $Z_{2D} = 2$ aggregates = 8 molecules). Aggregates from successive bilayers are respectively mirror images and placed on top of each other. The resulting cell of $P4/ncc$ symmetry involves 2 lamellae and $Z = 16$ molecules ($a = b = 27.4775 \text{ \AA}$, $c = 22.2649 \text{ \AA}$). This structure comes down to a supramolecular arrangement of strings of aggregates, the voids left at the interstices between strings explaining the relatively low density ($\rho = 1.162 \text{ g/cm}^3$), when compared to the structure of the **para-DSF-IDT** isomer ($\rho = 1.257 \text{ g/cm}^3$).

It should be mentioned that the confidence values for the structure refinements are good for **para-DSF-IDT**. Although logically less good than for the smaller cell of the *para* isomer, the refinement for **meta-DSF-IDT** is acceptable.

Thermal properties. The thermal properties of **para-** and **meta-DSF-IDT** were investigated by thermogravimetric analysis (TGA, see Figure S1 in SI) and differential scanning calorimetry (DSC, Figure 5). Both compounds possess high decomposition temperature, with T_d (5 % weight loss) of $323 \text{ }^\circ\text{C}$ for **para-DSF-IDT** and $339 \text{ }^\circ\text{C}$ for **meta-DSF-IDT**. These values show that the presence of the thienyl units has no strong influence on the thermal stability, compared to T_d reported for **[1,2-b]-DSF-IF** ($355 \text{ }^\circ\text{C}$)^[40] and **[2,1-a]-DSF-IF** ($330 \text{ }^\circ\text{C}$)^[41]. The high thermal stability is a characteristic of most of the 3π -2-spiro derivatives, however, one can note that the *para* isomer has a higher T_d in the IF series whereas the opposite is observed in the IDT series.

Physical properties of **para-DSF-IDT** and **meta-DSF-IDT** appear to be drastically different highlighting again the remarkable impact of positional isomerism not only on the electronic properties discussed below but also on the molecular packing. Indeed, **para-DSF-IDT** is a fine-crystalline powder for which optical microscopy revealed no textural change and DSC no phase transition (Figure 5, Left and Figure S2 in SI), up to $300 \text{ }^\circ\text{C}$. Consistently, SAXS patterns at room and at higher temperatures demonstrated the same crystalline state (Figure 6, left), and the structure is moreover the same as for the **para-DSF-IDT** single crystal (except the slightly larger lattice parameters due to the thermal expansion between the single crystal and SAXS pattern temperatures of respectively 150 K and ca. $20 \text{ }^\circ\text{C}$: $a = b = 21.72 \text{ \AA}$, $c = 8.70 \text{ \AA}$). The crude **meta-DSF-IDT** powder is a dark soft solid becoming pasty above $140 \text{ }^\circ\text{C}$, before its final melting to the isotropic liquid at around $160 \text{ }^\circ\text{C}$. Accordingly, DSC (Figure 5, right) shows several exothermic signals before endothermic melting peaks, which should come from several successive partial crystallization and recrystallization processes. This interpretation is confirmed by SAXS (Figure 6, right): the initial pattern at the room temperature is indicative of an amorphous state as it contains only broad signals from local-range interactions, which become overlapped with sharp reflections from the crystallized fraction upon heating at higher temperature. The presence of small reflections indicates a large-size cell that is however different from the crystal phase described above for the **meta-DSF-IDT** single crystals grown from solution. Since this latter phase includes rather large void zones, it can probably not be obtained from the molten bulk sample.

Figure 5. DSC of **para-DSF-IDT** (left) and **meta-DSF-IDT** (right)

Figure 6. SAXS patterns of *para*-DSF-IDT and *meta*-DSF-IDT in the pristine state (bottom, dark), on heating to $140 \text{ }^\circ\text{C}$ (red, middle) and on cooling to room temperature (blue, top).

The main physicochemical properties and theoretical calculations of **para-DSF-IDT** and **meta-DSF-IDT** are summarized in Table 1 together with those of **[1,2-b]-DSF-IF** and **[2,1-a]-DSF-IF**.

Table 1. Main photophysical properties of **para-DSF-IDT** and **meta-DSF-IDT** and of **[1,2-b]-DSF-IF** and **[2,1-a]-DSF-IF**

	$\lambda_{\text{ABS}} \text{ (nm)}^{\text{a}}$ $(\epsilon) (\times 10^4 \text{ L}\cdot\text{mol}^{-1}\cdot\text{cm}^{-1})$
	$\lambda_{\text{ABS}} \text{ (nm)}^{\text{b}}$
	$\lambda_{\text{EM}} \text{ (nm)}^{\text{a}}$
Quantum yield $\Phi^{\text{a,c}}$	
	$\lambda_{\text{EM}} \text{ (nm)}^{\text{b}}$
HOMO ^{el} /LUMO ^{el} / ΔE^{el} (eV) ^d	
	$\Delta E_{\text{Opt}}^{\text{e}}$ (eV)
	E_{T} (eV) ^f
HOMO ^{theo} /LUMO ^{theo} / ΔE^{theo} (eV)	-5.73/-1.37/4.36
	T_d (°C)

a: in cyclohexane, b. in thin film obtained by spin-coating from THF solution (10mg/10ml) c. calculated with reference to quinine sulfate in 1N H₂SO₄ ($\Phi=0.546$), d: from onset potentials, e: ΔE_{Opt} is calculated from the edge of the absorption spectrum using $\Delta E_{\text{Opt}}=hc/\lambda$, f. calculated with the first phosphorescent transition observed in a glassy matrix of methylcyclohexane/2-methylpentane (1/1) at 77K.

Electrochemical properties.

Electrochemical studies of **para**- and **meta**-DSF-IDT were performed in oxidation in Bu₄NPF₆ 0.2 M / CH₂Cl₂ solutions and in reduction in Bu₄NPF₆ 0.1 M / DMF solutions at concentrations around 2.10⁻³ M.

In oxidation, the two isomers present a different behavior as depicted on the cyclic voltammetry curves (CVs) presented figure 7. Two main differences are observed: (i) the onset oxidation potential is recorded at 0.70 V for **para**-DSF-IDT and at 0.9 V for **meta**-DSF-IDT, (ii) **para**-DSF-IDT presents four successive oxidation waves (with maxima recorded at 0.8, 1.37, 1.65 and 1.86 V) between 0.5 and 2.0 V vs SCE whereas **meta**-DSF-IDT only presents three oxidation waves (with maxima recorded at 0.99, 1.62 and 1.99 V) in the same potential range. It should be noted that the first oxidation of the spiro[fluorene-9,4'-[4H]indeno[3,2-b]thiophene] ('*spiro-FIT*', see structure in chart 1 in supplementary data), which can be roughly view as "the half" of the *meta*- or the *para*-DSF- IDTs, is reported in literature at more than 1.3 V vs SCE.^[64] Thus, the incorporation of an additional thienyl unit in the present IDT **meta**-DSF-IDT and **para**-DSF-IDT leads to an impressive decrease, ca >0.6 V of the first oxidation potential.

Figure 7. Cyclic voltammeteries (Bu₄NPF₆ 0.2 M / CH₂Cl₂, sweep-rate 100 mV s⁻¹, platinum disk working electrode, \varnothing 1 mm) in presence of **para**-DSF-IDT (in black) and **meta**-DSF-IDT (in red). Potential range: 0.25 to 2.25 V (Left) and 0.25 to 1.8 V (Right).

From the onset potentials, we determined the HOMO energy levels (HOMO(eV))= $-[E_{\text{onset}}^{\text{ox}}(\text{vs SCE})+4.4]$ ^[65] lying at -5.10 eV for **para**-DSF-IDT and at -5.30 eV for **meta**-DSF-IDT. These HOMO levels are remarkably higher than those of **[1,2-b]-DSF-IF** (-5.76 eV)^[51] and **[2,1-b]-DSF-IF** (-5.80 eV)^[39] analogues. This important feature clearly shows that the switching of the external phenyl units in the IF core by two thienyl units in the IDT core leads to a significant increase of the HOMO energy level of more than 0.5

eV (0.66 eV in the *para* series and 0.5 eV in the *meta*-series). This is caused by the electron rich character of the thienyl fragment, which has hence a strong influence on the HOMO energy level (theoretical calculations show that the HOMOs of **para**- and **meta**-DSF-IDT are spread out on the IDT core without any contribution of the fluorenyl cores, Figure 10). In addition, there is a 0.2 eV difference between the HOMO energy levels **para**-DSF-IDT and **meta**-DSF-IDT, which is assigned to the nature of the linkages.

Indeed, it is known that π -conjugation is maximized with *para* linkages and restricted in the case *meta* linkages^[39] (although, in the light of recent works,^[66] this general notion is not trivial). Herein, this π -conjugation disruption is clearly observed in the electronic distribution of the HOMO (and LUMO) of **meta**-DSF-IDT, which displays a nodal plane at the two opposite carbon atoms of the central phenyl ring (Figure 10). This feature, caused by the *meta* linkages, disrupts the π -conjugation of the IDT backbone and hence the HOMO energy level of **meta**-DSF-IDT is maintained at a lower energy than that of **para**-DSF-IDT. However, it is important to note that the magnitude is higher for **para**-DSF-IDT / **meta**-DSF-IDT (0.2 eV) than it was for **[1,2-b]-DSF-IF** / **[2,1-b]-DSF-IF** (0.04 eV).^[39, 51] Indeed, the thienyl ring is strongly less aromatic than the phenyl ring and therefore ensures a better delocalization

of π -electrons.^[67] The nature of the linkages has hence a stronger influence than in the case of phenyl rings, for which the electrons are more confined and hence less subjected to the delocalization. This is a significant difference between IF and IDT cores.

Looking more deeply at the successive first oxidation processes (Figure 7, Right) one can observe that for **para-DSF-IDT**, the two first oxidations are reversible whereas for **meta-DSF-IDT** only the first oxidation is reversible (for **para-** and **meta-DSF-IDT**, the third and second oxidations respectively are quasi-reversible). Differential Pulse Voltammetry (DPV) studies (Figure S27 in SI) show that the two first oxidations are quasi-iso-electronic for both compounds whereas the third oxidation of **para-DSF-IDT** is less intense than the two first ones. These two/three first oxidations have been attributed to the oxidation of the central IDT cores as they are reversible and occur in a potential range not sufficient to oxidize the fluorene cores. The oxidation of the fluorene cores are indeed observed in a more intense oxidation wave at higher potential values with peak potentials at 1.80 V for **para-DSF-IDT** and at 1.99 V for **meta-DSF-IDT**. Those potential values are in accordance with those observed for the fluorenyl units oxidation of the DSF-IF derivatives (around 1.95-1.99 V for **[1,2-b]-DSF-IF**^[51] and 1.94 V for **[2,1-b]-DSF-IF**^[39]). Moreover, reaching such high anodic values clearly leads to a polymerization process only involving the fluorene units (the coupling positions on the IDT cores are indeed blocked by the hexyl groups) as presented Figure 9 and discussed below.

In reduction, neither **para-DSF-IDT** nor **meta-DSF-IDT** present any distinguishable reduction wave before the accessible limit of the electrolytic solution in dichloromethane, the reduction was consequently studied in Bu₄NPF₆ 0.1 M in DMF (Figure 8).

The two isomers present between -1.0 and -3.0 V two reduction waves with maxima at -2.43 and -2.75 V for the **para-DSF-IDT** and at -2.6 and -2.8 V for the **meta-DSF-IDT**. For both compounds, a third reduction wave appears as a shoulder at the beginning of the electrolytic solution reduction (Figure S28 in SI). Looking at the differential pulse voltammograms (see DPV, Figure S29 in SI), it appears that for the two isomers the two first reduction waves are iso-electronic whereas the third one seems more intense. For both compounds, the first reduction is attributed to the reduction of the IDT cores whereas the second one at ca -2.75/-2.8 V is attributed to the reduction of the spiro-linked fluorene units. Indeed, this second wave is recorded in a potential range similar to that of the reduction of 9,9'-spirobifluorene^[51] (-2.73 V) or to that of the second reduction of DSF-IF derivatives.^[51]

Figure 8. Cyclic voltammograms (sweep-rate 100 mV s⁻¹) recorded in Bu₄NPF₆ 0.1 M / DMF, in presence of **para-DSF-IDT** (in black) and **meta-DSF-IDT** (in red) (platinum disk working electrode, \varnothing 1mm).

So, from the onset of the reduction potential (-2.31 V for **para-DSF-IDT** and at -2.48 V for **meta-DSF-IDT**), we determined the LUMO levels (LUMO(eV) = $-[E_{\text{onset}}^{\text{red}}(\text{vs SCE}) + 4.4]$ ^[65]) for the two compounds at -2.09 eV for **para-DSF-IDT** and -1.92 eV for **meta-DSF-IDT**. As reported for the HOMO, molecular modeling shows that the LUMO is mainly distributed on the IDT fragments with a clear conjugation breaking on the central phenyl ring in the case of the *meta*-IDT core (Figure 10).

Thus, the electrochemical energy gap ΔE_{El} ($\Delta E_{\text{El}} = \text{LUMO} - \text{HOMO}$) is evaluated at ca 3.01 eV for **para-DSF-IDT** and at 3.38 eV for the **meta-DSF-IDT**, these values being remarkably shorter than those of their DSF-IF analogues. Indeed, both **[1,2-b]-DSF-IF** and **[2,1-b]-DSF-IF** possess wide HOMO/LUMO differences, $\Delta E_{\text{El}} = 3.59/4.05$ eV respectively with HOMO/LUMO levels lying at -5.76/-2.17 eV **[1,2-b]-DSF-IF**^[40] and at -5.80/-1.75 eV for **[2,1-b]-DSF-IF**^[39]. We note however a similar difference in term of

ΔE_{El} between *para* and *meta* isomers (0.46 eV in the DSF-IF series and 0.37 eV in the DSF-IDT series).

Anodic deposition - synthesis of electroactive polymers.

Anodic polymerization is a powerful tool to generate electroactive oligomers or polymers for many applications,^[68] ranging from electrochromism^[69] to catalysis^[70-71] or sensors^[72]. Studying the electropolymerization of **para**- and **meta**-DSF-IDT appears hence as an interesting feature.

Figure 9. Cyclic voltammeteries (Bu₄NPF₆ 0.2 M / CH₂Cl₂, sweep-rate 100 mV s⁻¹, platinum disk working electrode) in presence of **para**-DSF-IDT (Left) and **meta**-DSF-IDT (Right) in concentration 1.88 10⁻³ M. Ten successive sweeps between 0.3 and 1.95 V (Left) or between 0.25 and 2.1 V (Right). The black arrows indicate the increase/decrease of the different waves along the 10 cycles.

As presented Figure 9, recurrent sweeps performed in a potential range including both the oxidation of the IDT cores and that of the spiro-linked fluorene units lead for the two compounds to a clear evolution of the CVs observed cycle after cycle and to the coverage of the electrode surface by an insoluble blue-black deposit named poly(**para**-DSF-IDT) or poly(**meta**-DSF-IDT) in the following discussion.

For **para**-DSF-IDT (Figure 9, left), ten cycles recorded between 0.3 and 1.95 V result in a regular increase of anodic and cathodic waves between 1.0 and 1.95 V and to the rapid disappearance of the **para**-DSF-IDT first oxidation wave E¹. Polymerization of **meta**-DSF-IDT is also observed along recurrent sweeps recorded between 0.25 and 2.1 V (Figure 9, right), however, the monomer first oxidation process E¹, observed at the first cycle, is shifted at potential higher than 1.25 V at the second sweep.

From the tenth CV, one may determine the onset oxidation potential of the deposits at 1.1 V for poly(**para**-DSF-IDT) and at 1.25 V for poly(**meta**-DSF-IDT) indicating HOMO levels of -5.50 eV and -5.65 eV for poly(**para**-DSF-IDT) and poly(**meta**-DSF-IDT) respectively. Despite that for **para**-DSF-IDT and **meta**-DSF-IDT, the polymerization process can only occur by fluorenyl-fluorenyl couplings (the coupling positions of the IDT cores are blocked by hexyl units), one observes that poly(**para**-DSF-IDT) and poly(**meta**-DSF-IDT) do not present the same HOMO energy level (HOMO of poly(**para**-DSF-IDT) at -5.50 eV and HOMO of poly(**meta**-DSF-IDT) at -5.65 eV). Interestingly, the 0.15 eV difference between the two deposit HOMO levels is comparable to that between the HOMO of their respective monomers (0.2 eV). Such a feature indicates the influence of the central IDT core on the electrochemical behavior of the electroactive deposits.

More surprising, the HOMO levels of the two deposits are deeper than that of their related monomers (-5.50 vs -5.10 eV for the *para* derivatives and -5.30 vs -5.65 eV for the *meta* derivatives). This uncommon feature is usually not observed for anodically generated polymers. Indeed, the rule is usually the following: HOMO_{monomer} < HOMO_{dimer} < HOMO_{trimer} <... < HOMO_{polymer} due to the conjugation extension.^[51-52, 73] Fluorene and polyfluorene (HOMO: -5.98 eV and -5.45 eV), dihydroindeno-1,2-b-fluorene (**1,2-b-IF**) and poly(**1,2-b-IF**) (HOMO: -5.62 eV and -5.17 eV)^[73], [**1,2-b**]-DSF-IF and poly([**1,2-b**]-DSF-IF) (HOMO: -5.76 eV and -5.34 eV, see Figure S30 in SI)^[51] **2,1-a-DSF-IF**^[35] and poly(**2,1-a-DSF-IF**) (see Figure S31 in SI) (HOMO: -5.64 eV and -5.55 eV) among others follow this rule.

We believe that the present feature, indicating the HOMO of the deposits deeper than the HOMO of the monomers, is caused by the nature of the coupling which takes place only between fluorenyl units and leads to oligofluorenes (dimer, trimer or higher oligomers) interlinked one to the others by dicationic IDT units (a mechanism of the polymerization process is suggested in Figure S32 in supplementary data). Indeed, the HOMOs of a fluorenyl dimer, a fluorenyl trimer and of the derived polyfluorene have been evaluated at -5.55, -5.49 and -5.45 eV respectively^[74] being hence similar to the HOMO of the present deposit (-5.50 and -5.65 eV *resp.*). We hence believe that the present deposits display between DSF-IDT units very short fluorenyl chains (dimers or trimers).

Finally it is also important to mention that at the E¹ potential (0.8 V for **para**-DSF-IDT and 0.99 V for **meta**-DSF-IDT), at which the IDT first oxidation occurs, the deposits are non-doped and therefore non-conducting avoiding any charge transfer from electrode to solution. The charge transfer becomes possible only when the deposit is oxidized (around 1.1 and 1.25 V for the poly(**para**-DSF-IDT) and at 1.25 V for the poly(**meta**-DSF-IDT)). This feature is not observed for poly(DSF-IF) derivatives, (Figures S29 and S30 in SI), for which the oxidation of the central dihydroindeno-fluorenyl cores (E¹ potentials of 1.4 V for [**1,2-b**]-DSF-IF and 1.55 V for [**2,1-b**]-DSF-IF) occurs when the deposits are under their p-doped forms (E_{onset}^{ox}: 0.94 V for the poly([**1,2-b**]-DSF-IF) and 1.15 V for the poly([**2,1-b**]-DSF-IF)) and are therefore conducting.

Theoretical calculations

Figure 10. Calculated frontier molecular orbitals of **para**-DSF-IDT (left) and **meta**-DSF-IDT (right), after geometry optimization with DFT B3LYP/6-311G+(d,p) shown with a cut-off 0.04 [e bohr⁻³]^{1/2}

Geometry optimization of the two isomers in the singlet state was performed using density functional theory (DFT) at the Gaussian 09 B3LYP/6-311+G(d,p) level of theory (Figure 10). The electronic distribution and the energy levels have been determined on optimized geometries. The calculated HOMO level of **para**-DSF-IDT (-5.11 eV) is higher than that of **meta**-DSF-IDT (-5.23 eV). The difference between these two values, 0.12 eV, is slightly larger than that calculated between the HOMO of the [**1,2-b**]- and [**2,1-b**]-DSF-IF (0.05 eV) and hence in accordance with the experimental electrochemical values above discussed. The calculated LUMO levels lie at -1.47 eV and -1.27 eV respectively for the **para**- and **meta**-DSF-IDT, leading to an energy gap of 3.64 eV and of 3.96

eV respectively. Thus, we note a gap contraction of 0.32 eV between the *para*- and the *meta*-isomer which appears slightly smaller than that obtained by electrochemical studies (0.37 eV).

Optical properties

Figure 11. UV-Vis absorption spectra (Left) and emission spectra (Right) of **para-DSF-IDT** (black line) and **meta-DSF-IDT** (red line) in cyclohexane. $\lambda_{\text{exc}} = 358$ nm for **para-DSF-IDT** and 345 nm for **meta-DSF-IDT**

The absorption spectrum of **para-DSF-IDT** recorded in cyclohexane presents between 250 and 450 nm four main bands (maxima at 266, 340, 357 and 376 nm, Figure 11, Left, black line), whereas that of **meta-DSF-IDT** is blue-shifted by around 13 nm and presents a more complicated spectrum with seven maxima (at 261, 273, 293, 304, 321, 345 and 363 nm, Figure 11, Left, red line). Thus, the nature of the linkages has a significant impact on the absorption maximum, which is the consequence of a better delocalization of π -electrons in **para-DSF-IDT** compared to **meta-DSF-IDT**. This 'linkage effect' remains classical but its magnitude appears unusual. Indeed, in the DSF-IF series, there was only a small difference of 1.5 nm between the absorption maximum of *para*- and *meta*-substituted isomers ($\lambda_{\text{max}} = 344$ nm for **[1,2-b]-DSF-IF**^[40] and 342.5 nm for **[2,1-b]-DSF-IF**^[42]). In the present case of IDT, the magnitude is impressively larger, ie 13 nm and is assigned to the presence of the bridged thienyl units. Indeed, as above mentioned the thienyl ring is strongly less aromatic than the phenyl ring and therefore ensures a better delocalization of π -electrons.^[67] Thus, with a *para* linkage, which strongly favors the π -delocalization,^[44, 47] there is an impressive red shift of 32 nm of the absorption maximum between **para-DSF-IDT** and **[1,2-b]-DSF-IF**. In the *meta* series, the red shift between the absorption maximum of **meta-DSF-IDT** and that of **[2,1-b]-DSF-IF** remains intense, 21 nm. Thus, due to the different aromaticity of thienyl vs phenyl rings, the nature of the linkage has a more important effect in the IDT series than in the IF one and allows therefore to finely tune the optical properties of the formers. For both isomers, absorption spectra remained similar whatever the solvent indicating no solvatochromic effect (Figure S32-33 in SI).

Optical energy gaps ΔE_{opt} (determined from the onset of the lowest energy absorption bands) were evaluated at ca. 3.21 and 3.36 eV for **para-DSF-IDT** and **meta-DSF-IDT** respectively. Such difference was not observed in the DSF-IF series, which possess an almost identical ΔE_{opt} of 3.53/3.55 eV for **[1,2-b]-DSF-IF**^[40]/ **[2,1-b]-DSF-IF**^[42]. Thus, modifying the linkages of the IDT backbone appears as an interesting strategy to significantly modulate their electronic properties. It should be mentioned that the energy gap difference between the isomers obtained from optical experiments: 0.15 eV is smaller than that obtained by electrochemistry or theoretical calculations (0.37 eV and 0.32 eV resp.) but the trend is the same.

Time-dependent density functional theory (TD-DFT) were also carried out for both compounds (RB3LYP TD-FC using 6-311+G(d,p)). As presented by the calculated UV-vis spectra of the two compounds (Figure 12, Middle), the lowest energy bands are red shifted by 27 nm from *meta*- to *para*-DSF-IDT (350 nm to 377 nm, in accordance with the 13 nm shift obtained from experimental UV-vis spectra (Figure 11, Left).

For **para-DSF-IDT** (Figure 12, Left), the first absorption band is assigned to a single HOMO-LUMO transition (377.57 nm, f: 0.7431) whereas for **meta-DSF-IDT** (Figure 12, Right), the absorption band centered at 350 nm includes three transitions: a HOMO-LUMO transition with a weak oscillator strength (351.89 nm, f: 0.0653), a HOMO-LUMO+2 transition with an intense oscillator strength (350.67 nm, f: 0.3326) and a HOMO-LUMO+3 with an even weaker oscillator strength (350.13 nm, f: 0.0083). For both compounds, the more intense transition of lower energy at 377.57 nm for **para-DSF-IDT** and at 350.67 nm for **meta-DSF-IDT** involve only the IDT cores (HOMO-LUMO for **para-DSF-IDT** and HOMO-LUMO+2 for **meta-DSF-IDT**). Thus, it should be stressed out that for the **meta-DSF-IDT**, the main transition is not a HOMO-LUMO transition as often observed for organic semiconductors and as observed for **para-DSF-IDT**. This is again a noticeable difference between the two isomers due to the different linkages.

Other transitions involving the IDT core are calculated for both compounds but transitions involving the fluorenyl units are only calculated for the **para-DSF-IDT** (284 nm, HOMO-1/LUMO+2 and HOMO-1/LUMO+1, Figure 12, left). It should be indeed mentioned that the HOMO-1 of **para-DSF-IDT** and **meta-DSF-IDT** appears different, one being spread out on the two fluorenyl cores (**para-DSF-IDT**) and the other being spread out on IDT core (**meta-DSF-IDT**).

Figure 12. Theoretical UV spectra (inset) and representation of the energy levels and the main molecular orbitals involved in the electronic transitions of **para-DSF-IDT** (left) and **meta-DSF-IDT** (middle) obtained by TD-DFT B3LYP/6-311G+(d,p) shown with an isovalues of 0.04 [$e \text{ bohr}^{-3}$]^{1/2}

The fluorescence spectra of both isomers recorded in cyclohexane presents a similar shape with a first band detected at 365 nm for **meta-DSF-IDT** and at 383 nm for **para-DSF-IDT** (Figure 11, Right). As observed in absorption spectroscopy, we note a similar red shift between the *meta* and *para* isomer (13 nm in absorption and 18 nm in emission). These well-resolved spectra are the mirror images of the corresponding absorption spectra (see zoom in the 330 and 450 nm region in Figure 11, Left) with Stokes shifts ($\lambda_{\text{em}} - \lambda_{\text{abs}}$ in nm) of 7 nm for **para-DSF-IDT** and of only 2 nm for **meta-DSF-IDT**, indicating a very weak reorganization between the S_0 and S_1 states for both isomers which are indeed very rigid molecules. Thus, the emission of both isomers results from their corresponding central IDT core. However, it should be noted that **meta-DSF-IDT** presents a larger Stokes shift than that of its *para* isomer. In the IF series, in which the emission comes from the central IF core, the same Stokes shift trend was observed but with a different magnitude, 2 nm for **[1,2-b]-DSF-IF** and 4 nm for **[2,1-b]-DSF-IF**. The quantum yield, Φ , (determined in cyclohexane

solutions with quinine sulfate in 1N H₂SO₄ as reference) is ca 0.26 for **para-DSF-IDT** and of ca 0.33 for **meta-DSF-IDT**. Both quantum yields are lower than those reported for **[1,2-b]-DSF-IF**^[51] (ca 0.62) and **[2,1-b]-DSF-IF**^[39] (ca 0.54). At this stage, it is difficult to assign with a complete certitude the quantum yield decrease and the different Stokes shifts to a precise feature as it may come either from the IDT backbone or to the alkyl chains. However, as another DSF-IF derivative has previously been reported in literature with octyl chains attached to the IF core^[50-51] without any drop of the quantum yield, we believe that in the present case the thienyl ring is responsible of the quantum yield decrease. For both isomers, emission spectra remained clearly similar (Figures S33- S34 in SI) whatever the solvent used (no photo induced intramolecular charge transfer).

In the solid state (films were spin-coated from THF at a concentration of 10 mg/mL), the absorption spectra of both **para-DSF-IDT** and **meta-DSF-IDT** remain structured with maxima recorded at 383 and 368 nm respectively, slightly shifted compared to those in solution (376 and 363 nm respectively). This means that the molecules do not strongly stack in thin film and this feature is hence in accordance with the crystal packing above described. This is caused by the presence of the bulky spirofluorenyl units which hinder strong intermolecular interactions. In fluorescence, we note a more intense red shift compared to the solution spectra (387/372 nm in thin film vs 383/365 nm in solution for **para-DSF-IDT/meta-DSF-IDT**) and the a more intense emission in the 450-550 nm range, meaning that the fluorescence is more influenced by the environment effects than the absorption. In order to perfectly unravel the solid-state fluorescence, more spectroscopic experiments would be necessary.

Figure 13. Normalized absorption (left) and emission spectra of spin-coated films (from THF at a concentration of 10mg/mL) of **meta-DSF-IDT** (red line, λ_{exc} =362 nm) and **para-DSF-IDT** (black line, λ_{exc} =352 nm)

Investigation of the properties of triplet state have finally been performed. Indeed, it has been recently shown that singlet and triplet states can follow different trends.^[47]

Figure 14. Emission spectra at 77K of **para-DSF-IDT** (black line) and **meta-DSF-IDT** (red line) in 2-Me-THF

At 77 K, the emission spectra of the two DSF-IDT isomers present different shapes (Figure 14). For **meta-DSF-IDT**, the phosphorescence contribution is constituted of several emission bands observed between 520 and 620 nm. Its E_T value, obtained by the highest-energy phosphorescent peak recorded at 528 nm, is estimated to lie at ca 2.35 eV. The phosphorescence contribution of **para-DSF-IDT** is broad with a maximum at 587 nm, giving an E_T value evaluated close to 2.12 eV. This E_T value is smaller than the one of the *meta*-isomer as it was the case for the DSF-IF derivatives (E_T: 2.76 eV for **[2,1-b]-DSF-IF**^[40] and 2.52 eV for **[1,2-b]-DSF-IF**^[40]). This is in accordance with a higher E_T value for the less conjugated *meta*-isomers compared to the more conjugated *para*- isomers. The difference between the two first transitions (and hence the difference of E_T) in the DSF-IDT and the DSF-IF series is similar (around 0.2 eV). We can hence conclude that the linkage effects are identical in the two series at 77K. This was not the case at room temperature in which the linkage effects were more important for the IDT series (18 nm shift from *meta* to *para*) than for the IF series (no shift). As main red phosphorescent dyes possess E_T around 2.0 eV,^[75] both **para-** and **meta-DSF-IDT** should be adapted to host red phosphorescent dyes, this will be performed in due course.

Conclusion

Thanks to a structure properties relationship approach, we report herein the first studies on the intrinsic properties of the dihydroindacenodithienyl fragment with a central *para*- or *meta*-phenyl/thienyl linkage and more generally we show the strong impact of positional isomerism on the IDT backbones. The strong influence of the *para*- and *meta*- linkages has been highlighted not only on the electronic properties in solution (HOMO/LUMO energy levels, optical transitions, fluorescence spectra...) but also on the physical properties in the solid state (phase transitions and crystallinity). The influence of the incorporation of the electron rich bridged thiophene units has also been compared to structurally related DSF-IFs possessing a dihydroindenofluorenyl core. Thus, at room temperature, it has been shown that the linkage effects are more pronounced for the IDT series (for both *para* and *meta* linkages) than for the IF series. However, at 77 K, it has been shown that the thienyl ring is strongly less influent.

Molecular architecture of the monomers has also an impact on the anodic polymerization process. We pointed that despite the IDT units cannot be involved in the main polymer skeleton (carbon-carbon bonds are not formed between IDT units but only between fluorenyl units), the electrochemical behavior of the derived polymer is influenced by the geometry of the IDT cores with an onset potential of the p-doping process lower for the poly(**para-DSF-IDT**) than for the poly(**meta-DSF-IDT**).

Thus, modifying the central phenyl linkages appears an efficient strategy (even more efficient than for DSF-IF) to tune the physical/electronic properties of IDT derivatives and highlights how positional isomerism can be an effective tool for such purpose. The next step will be to incorporate these molecules in judiciously designed electronic devices and we are currently working in this direction.

Acknowledgments.

We thanks the CDFIX (Rennes) for X-ray analyses, the C.R.M.P.O (Rennes) for mass analyses, Région Bretagne and the Agence de l'Environnement et de la Maîtrise de l'Energie (ADEME) for a studentship (JDP), Dr Bruno Laffite (ADEME). This work was

granted access to the computing resources of CINES (Montpellier, allocation 2017-A0020805032 awarded by GENCI). BD and BH thank the CNRS and Université de Strasbourg (UNISTRA) for support.

References

- [1] J.-H. Jou, S. Kumar, A. Agrawal, T.-H. Li and S. Sahoo, *J. Mater. Chem. C* **2015**, *3*, 2974-3002.
- [2] H. Sasabe and J. Kido, *Eur. J. Org. Chem.* **2013**, 7653–7663.
- [3] Y. Tao, C. Yang and J. Qin, *Chem. Soc. Rev.* **2011**, *40*, 2943-2970.
- [4] L. Xiao, Z. Chen, B. Qu, J. Luo, S. Kong, Q. Cong and J. Kido, *Adv. Mater.* **2011**, *23*, 926-952.
- [5] K. S. Yook and J. Y. Lee, *Chem. Rec.* **2016**, *16*, 159-172.
- [6] D. Volz, *J. Photon. Energy* **2016**, *6*, 020901-020901.
- [7] Y. Im, S. Y. Byun, J. H. Kim, D. R. Lee, C. S. Oh, K. S. Yook and J. Y. Lee, *Adv. Funct. Mater.* **2017**, *27*, 1603007.
- [8] X. Xu, X. Yang, J. Zhao, G. Zhou and W.-Y. Wong, *Asian J. Org. Chem.* **2015**, *4*, 394-429.
- [9] X. Gao and Z. Zhao, *Sc. China Chem.* **2015**.
- [10] Q. Meng and W. Hu, *Phys. Chem. Chem. Phys.* **2012**, *14*, 14152–14164.
- [11] A. Facchetti, *Materials Today* **2007**, *10*, 28-37.
- [12] J. W. Ward, Z. A. Lampion and O. D. Jurchescu, *ChemPhysChem* **2015**, *16*, 1118-1132.
- [13] G. Luo, X. Ren, S. Zhang, H. Wu, W. C. H. Choy, Z. He and Y. Cao, *Small* **2016**, *12*, 1547-1571.
- [14] H. Youn, H. J. Park and L. J. Guo, *Small* **2015**, *11*, 2228-2246.
- [15] K. A. Mazzi and C. K. Luscombe, *Chem. Soc. Rev.* **2015**, *44*, 78-90.
- [16] K. Nakano and K. Tajima, *Adv. Mater.* **2016**, 1-33.
- [17] C. Li, M. Liu, N. G. Pschirer, M. Baumgarten and K. Müllen, *Chem. Rev.* **2010**, *110*, 6817–6855.
- [18] J.-L. Wang, K.-K. Liu, J. Yan, Z. Wu, F. Liu, F. Xiao, Z.-F. Chang, H.-B. Wu, Y. Cao and T. P. Russell, *J. Am. Chem. Soc.* **2016**, *138*, 7687-7697.
- [19] Y. Lin, Q. He, F. Zhao, L. Huo, J. Mai, X. Lu, C.-J. Su, T. Li, J. Wang, J. Zhu, Y. Sun, C. Wang and X. Zhan, *J. Am. Chem. Soc.* **2016**, *138*, 2973-2976.
- [20] E. Y. Ko, G. E. Park, J. H. Lee, H. J. Kim, D. H. Lee, H. Ahn, M. A. Uddin, H. Y. Woo, M. J. Cho and D. H. Choi, *ACS Appl. Mater. Interfaces* **2017**, *9*, 8838-8847.
- [21] J.-L. Wang, F. Xiao, J. Yan, K.-K. Liu, Z.-F. Chang, R.-B. Zhang, H.-B. Wu and Y. Cao, *J. Mater. Chem. A* **2016**, *4*, 2252-2262.
- [22] J.-L. Wang, Q.-R. Yin, J.-S. Miao, Z. Wu, Z.-F. Chang, Y. Cao, R.-B. Zhang, J.-Y. Wang, H.-B. Wu and Y. Cao, *Adv. Funct. Mater.* **2015**, *25*, 3514-3523.
- [23] H. Tian, Y. Deng, F. Pan, L. Huang, D. Yan, Y. Geng and F. Wang, *J. Mater. Chem.* **2010**, *20*, 7998-8004.
- [24] B. S. Young, D. T. Chase, J. L. Marshall, C. L. Vonnegut, L. N. Zakharov and M. M. Haley, *Chem. Sci.* **2014**, *5*, 1008-1014.
- [25] I. Isakov, A. F. Paterson, O. Solomeshch, N. Tessler, Q. Zhang, J. Li, X. Zhang, Z. Fei, M. Heeney and T. D. Anthopoulos, *Appl. Phys. Lett.* **2016**, *109*, 263301.
- [26] H. Bronstein, D. S. Leem, R. Hamilton, P. Woebkenberg, S. King, W. Zhang, R. S. Ashraf, M. Heeney, T. D. Anthopoulos, J. de Mello and I. McCulloch, *Macromolecules* **2011**, *44*, 6649-6652.
- [27] M. Planells, M. Nikolka, M. Hurhangee, P. S. Tuladhar, A. J. P. White, J. R. Durrant, H. Siringhaus and I. McCulloch, *J. Mater. Chem. C* **2014**, *2*, 8789-8795.
- [28] X. Zhang, H. Bronstein, A. J. Kronemeijer, J. Smith, Y. Kim, R. J. Kline, L. J. Richter, T. D. Anthopoulos, H. Siringhaus, K. Song, M. Heeney, W. Zhang, I. McCulloch and D. M. DeLongchamp, *Nat. Commun.* **2013**, *4*, 2238.
- [29] W. Zhang, J. Smith, S. E. Watkins, R. Gysel, M. McGehee, A. Salleo, J. Kirkpatrick, S. Ashraf, T. Anthopoulos, M. Heeney and I. McCulloch, *J. Am. Chem. Soc.* **2010**, *132*, 11437-11439.
- [30] Y. Li, M. Gu, Z. Pan, B. Zhang, X. Yang, J. Gu and Y. Chen, *J. Mater. Chem. A* **2017**, *5*, 10798-10814.
- [31] K.-T. Wong, T.-C. Chao, L.-C. Chi, Y.-Y. Chu, A. Balaiah, S.-F. Chiu, Y.-H. Liu and Y. Wang, *Org. Lett.* **2006**, *8*, 5033-5036.
- [32] J.-D. Peltier, B. Heinrich, B. Donnio, J. Rault-Berthelot, E. Jacques and C. Poriel, *ACS Appl. Mater. Interfaces* **2017**, *9*, 8219-8232.
- [33] C. Poriel, J. Rault-Berthelot, F. Barrière and A. M. Z. Slawin, *Org. Lett.* **2008**, *10*, 373-376.
- [34] D. Thirion, C. Poriel, F. Barrière, R. Métivier, O. Jeannin and J. Rault-Berthelot, *Org. Lett.* **2009**, *11*, 4794-4797.
- [35] D. Thirion, C. Poriel, J. Rault-Berthelot, F. Barrière and O. Jeannin, *Chem. Eur. J.* **2010**, *16*, 13646-13658.
- [36] C. Poriel, R. Métivier, J. Rault-Berthelot, D. Thirion, F. Barrière and O. Jeannin, *Chem. Commun.* **2011**, *47*, 11703-11705.
- [37] C. Poriel, N. Cocherel, J. Rault-Berthelot, L. Vignau and O. Jeannin, *Chem. Eur. J.* **2011**, *17*, 12631-12645.
- [38] D. Thirion, M. Romain, J. Rault-Berthelot and C. Poriel, *J. Mater. Chem.* **2012**, *22*, 7149-7157.
- [39] M. Romain, D. Tondelier, J.-C. Vanel, B. Geffroy, O. Jeannin, J. Rault-Berthelot, R. Métivier and C. Poriel, *Angew. Chem Int. Ed.* **2013**, *52*, 14147–14151.

- [40] M. Romain, S. Thiery, A. Shirinskaya, C. Declairieux, D. Tondelier, B. Geffroy, O. Jeannin, J. Rault-Berthelot, R. Métivier and C. Poriel, *Angew. Chem Int. Ed.* **2015**, *54*, 1176-1180.
- [41] M. Romain, D. Tondelier, B. Geffroy, O. Jeannin, E. Jacques, J. Rault-Berthelot and C. Poriel, *Chem. Eur. J.* **2015**, *21*, 9426-9439.
- [42] M. Romain, C. Quinton, D. Tondelier, B. Geffroy, O. Jeannin, J. Rault-Berthelot and C. Poriel, *J. Mater. Chem. C* **2016**, *4*, 1692-1703.
- [43] S. Thiery, D. Tondelier, C. Declairieux, B. Geffroy, O. Jeannin, R. Métivier, J. Rault-Berthelot and C. Poriel, *J. Phys. Chem. C* **2015**, *119*, 5790-5805.
- [44] L. Sicard, C. Quinton, J.-D. Peltier, D. Tondelier, B. Geffroy, U. Biapo, R. Métivier, O. Jeannin, J. Rault-Berthelot and C. Poriel, *Chem. Eur. J.* **2017**, *23*, 7719-7727.
- [45] S. Thiery, B. Heinrich, B. Donnio, C. Poriel and F. Camerel, *J. Phys. Chem. C* **2015**, *119*, 10564-10575.
- [46] S. Thiery, C. Declairieux, D. Tondelier, G. Seo, B. Geffroy, O. Jeannin, R. Métivier, J. Rault-Berthelot and C. Poriel, *Tetrahedron* **2014**, *70*, 6337-6351.
- [47] C. Poriel and J. Rault - Berthelot, *J. Mater. Chem. C* **2017**, *5*, 3869-3897
- [48] D. Thirion, C. Poriel, R. Métivier, J. Rault-Berthelot, F. Barrière and O. Jeannin, *Chem. Eur. J.* **2011**, *17*, 10272-10287.
- [49] C. Poriel, J. Rault-Berthelot, D. Thirion, F. Barrière and L. Vignau, *Chem. Eur. J.* **2011**, *17*, 14031-14046.
- [50] D. Horhant, J.-J. Liang, M. Virboul, C. Poriel, G. Alcaraz and J. Rault-Berthelot, *Org. Lett.* **2006**, *8*, 257-260.
- [51] C. Poriel, J.-J. Liang, J. Rault-Berthelot, F. Barrière, N. Cocherel, A. M. Z. Slawin, D. Horhant, M. Virboul, G. Alcaraz, N. Audebrand, L. Vignau, N. Huby, G. Wantz and L. Hirsch, *Chem. Eur. J.* **2007**, *13*, 10055-10069.
- [52] N. Cocherel, C. Poriel, J. Rault-Berthelot, F. Barrière, N. Audebrand, A. M. A. Slawin and L. Vignau, *Chem. Eur. J.* **2008**, *14*, 11328-11342.
- [53] N. Cocherel, C. Poriel, L. Vignau, J.-F. Bergamini and J. Rault-Berthelot, *Org. Lett.* **2010**, *12*, 452-455. [54] D. Thirion, J. Rault-Berthelot, L. Vignau and C. Poriel, *Org. Lett.* **2011**, *13*, 4418-4421.
- [55] E. Jacques, M. Romain, A. Yassin, S. Bebiche, M. Harnois, T. Mohammed-Brahim, J. Rault-Berthelot and C. Poriel, *J. Mater. Chem. C* **2014**, *2*, 3292-3302.
- [56] M. Romain, M. Chevrier, S. Bebiche, T. Mohammed-Brahim, J. Rault-Berthelot, E. Jacques and C. Poriel, *J. Mater. Chem. C* **2015**, *3*, 5742-5753.
- [57] C. Poriel, F. Barrière, D. Thirion and J. Rault-Berthelot, *Chem. Eur. J.* **2009**, *15*, 13304-13307.
- [58] H. Bronstein, D. S. Leem, R. Hamilton, P. Woebkenberg, S. King, W. Zhang, R. S. Ashraf, M. Heeney, T. D. Anthopoulos, J. de Mello and I. McCulloch, *Macromolecules* **2011**, *44*, 6649-6652.
- [59] T. Nakano and T. Yade, *J. Am. Chem. Soc.* **2003**, *125*, 15474-15484.
- [60] Y. Ting and Y.-H. Lai, *J. Am. Chem. Soc.* **2004**, *126*, 909-914.
- [61] X. Mei and C. Wolf, *J. Org. Chem.* **2005**, *70*, 2299-2305.
- [62] R. Rathore, S. H. Abdelwahed and I. A. Guezi, *J. Am. Chem. Soc.* **2003**, *125*, 8712-8713.
- [63] Wang W.L., Xu J., Sun Z., Zhang X., Lu Y. and L. Y.-H., *Macromolecules* **2006**, *39*, 7277-7285.
- [64] T. Kowada, Y. Matsuyama and K. Ohe, *Synlett* **2008**, *2*, 1902-1906.
- [65] A. P. Kulkarni, C. J. Tonzola, A. Babel and S. A. Jenekhe, *Chem. Mater.* **2004**, *16*, 4556-4573.
- [66] K. Amro, A. K. Thakur, J. Rault-Berthelot, C. Poriel, L. Hirsch, W. E. Douglas, S. Clement and P. Gerbier, *New J. Chem.* **2013**, *37*, 464-473.
- [67] Z.-G. Zhang and J. Wang, *J. Mater. Chem.* **2012**, *22*, 4178-4187.
- [68] J. Heinze, B. A. Frontana-Urbe and S. Ludwigs, *Chem. Rev.* **2010**, *110*, 4724-4771.
- [69] P. M. Beaujuge and J. R. Reynolds, *Chem. Rev.* **2010**, *110*, 268-320.
- [70] C. Poriel, Y. Ferrand, P. Le Maux, J. Rault-Berthelot and G. Simonneaux, *Inorg. Chem.* **2004**, *43*, 5086-5095.
- [71] Y. Ferrand, C. Poriel, P. Le Maux, J. Rault-Berthelot and G. Simonneaux, *Tetrahedron: Asymmetry* **2005**, *16*, 1463- 1472.
- [72] C. Paul-Roth, J. Rault-Berthelot, G. Simonneaux, C. Poriel, M. Abdalilah and J. Letessier, *J. Electroanal. Chem.* **2006**, *597*, 19-27.
- [73] J. Rault-Berthelot, C. Poriel, F. Justaud and F. Barrière, *New J. Chem.* **2008**, *32*, 1259-1266.
- [74] P. Hapiot, C. Lagrost, F. Le Floch, E. Raoult and J. Rault-Berthelot, *Chem. Mater.* **2005**, *17*, 2003-2012.
- [75] J.-H. Kwon and R. Pode in *High Efficiency Red Phosphorescent Organic Light-Emitting Diodes with Simple Structure*, (Ed. S. H. Ko), InTech, Rijeka, **2011**, p. Ch. 04.

Modulating the physical and electronical properties over positional isomerism: the Dispirofluorene-Dihydroindacenodithiophene (DSF-IDT) family.

Jean-David Peltier,^a Benoît Heinrich,^b Bertrand Donnio,^b Olivier Jeannin,^a Joëlle Rault-Berthelot,^{a*} Cyril Poriel^{a*}

^a UMR CNRS 6226-ISCR-Université de Rennes 1-35042 Rennes cedex-France

^b Institut de Physique et Chimie des Matériaux de Strasbourg, UMR 7504, CNRS-Université de Strasbourg, 23 rue du Loess, BP 43, 67034, Strasbourg Cédex 2 France

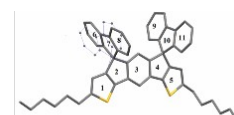
E-mail: cyril.poriel@univ-rennes1.fr, joelle.rault@univ-rennes1.fr

Abstract

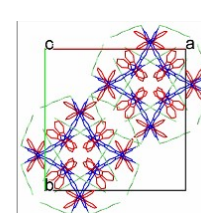
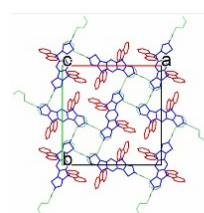
We report the first studies on the intrinsic properties of a *meta*-substituted dihydroindacenodithienyl fragment and more generally the strong impact of positional isomerism on dihydroindacenodithiophene derivatives. The influence of the *para* and *meta* linkages has notably been highlighted not only on the electronic properties in solution (electrochemical properties, anodic polymerization, HOMO/LUMO energy levels, optical transitions, fluorescence spectra...) but also on the physical properties in the solid state (molecular organization, crystallinity and phase transitions). The positional isomerism hence appears as a very efficient tool to drastically tune the properties of dihydroindacenodithiophene derivatives.



Para-DSF-IDT



Meta-DSF-IDT



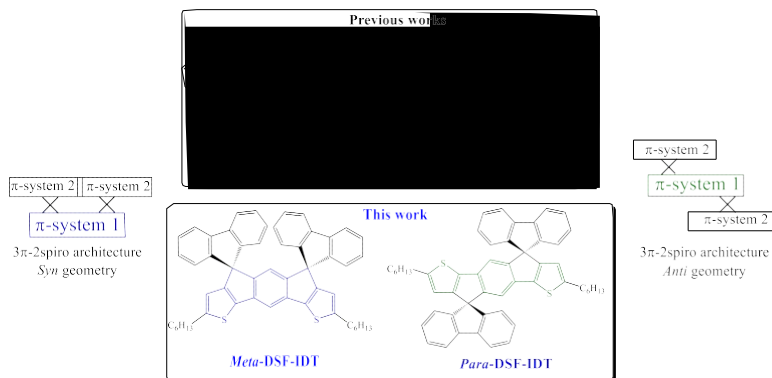
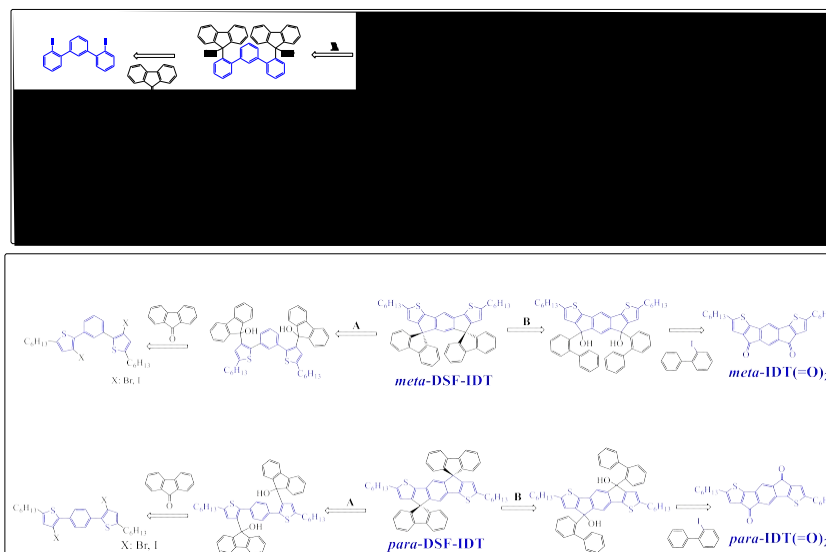
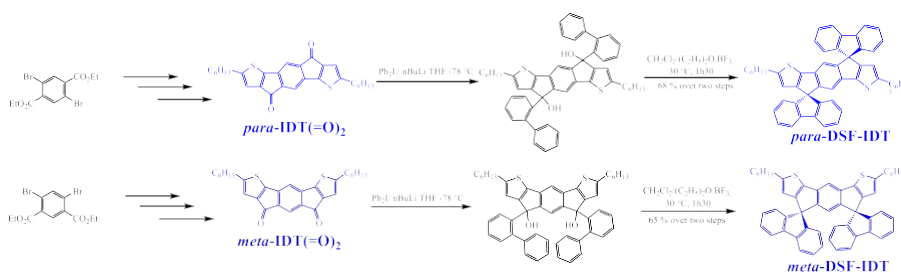


Figure 1: Dihydroindacenodithienyl derivatives **meta**-DSF-IDT and **para**-DSF-IDT investigated in this work and their pure hydrocarbon analogues [1,2-*b*]-DSF-IF⁴⁸ and [2,1-*b*]-DSF-IF⁴²



Scheme 1. Retrosynthetic approaches to DSF-IF and DSF-IDT



Scheme 2. Synthesis of **para**-DSF-IDT and **meta**-DSF-IDT

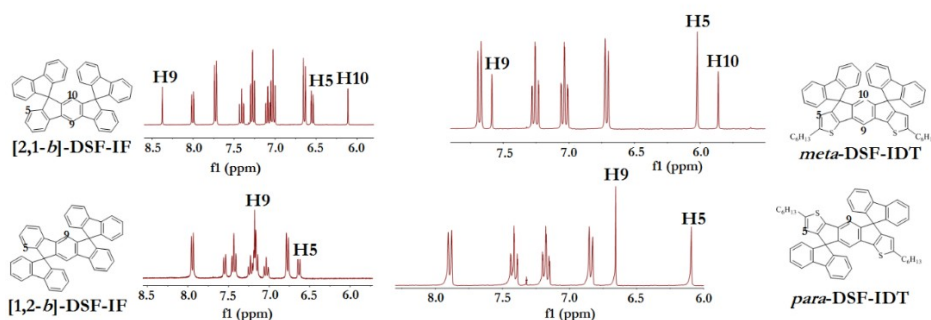


Figure 2. A portion of ¹H NMR spectra (CD₂Cl₂) of left : [2,1-*b*]-DSF-IF (top) and [1,2-*b*]-DSF-IF (bottom) and right : **para**-DSF-IDT (top) and **meta**-DSF-IDT (bottom).

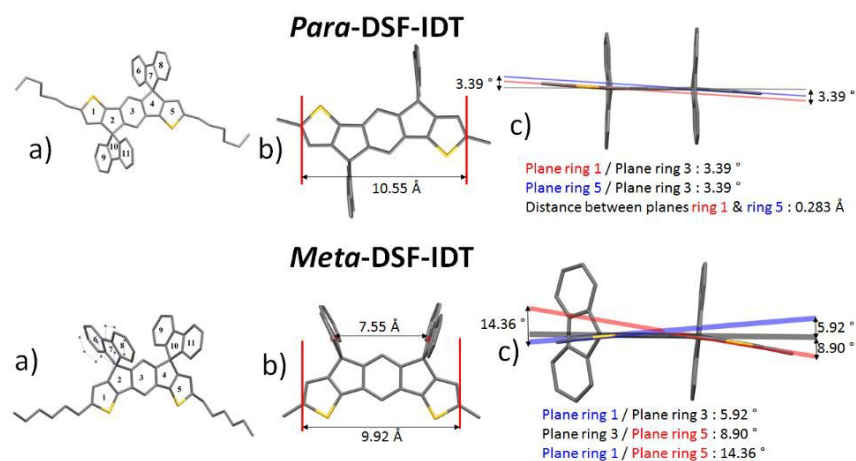


Figure 3. Molecular structures from X-ray crystallography of **para-DSF-IDT** (top) and **meta-DSF-IDT** (bottom). The hydrogen atoms have been omitted for clarity. In b) and c), the hexyl chains have been reduced to methyl groups for purpose of clarity.

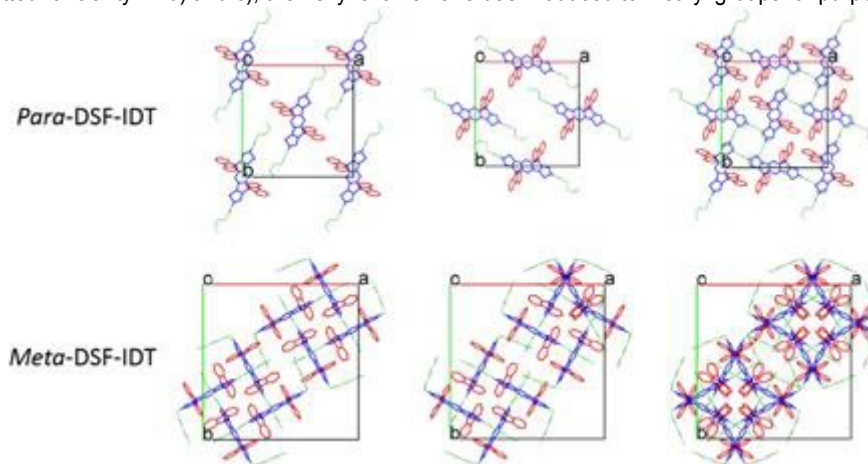


Figure 4. Crystal packing in the **a**×**b** planes obtained from X-ray crystallography of **para-DSF-IDT** (top) and **meta-DSF-IDT** (bottom). Left: top monolayer, middle: bottom layer and right all the layers. The hydrogen atoms have been omitted for clarity, in blue the IDT cores, in red the fluorenes and in green the alkyl chains.

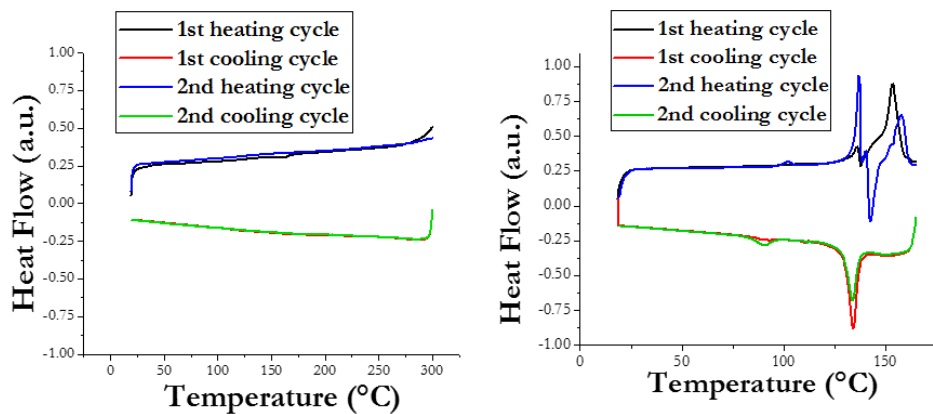


Figure 5. DSC of **para-DSF-IDT** (left) and **meta-DSF-IDT** (right)

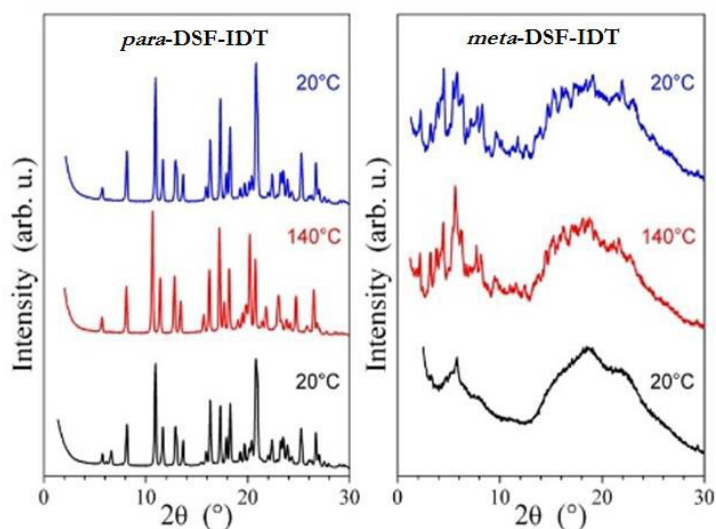


Figure 6. SAXS patterns of *para*-DSF-IDT and *meta*-DSF-IDT in the pristine state (bottom, dark), on heating to 140°C (red, middle) and on cooling to room temperature (blue, top).

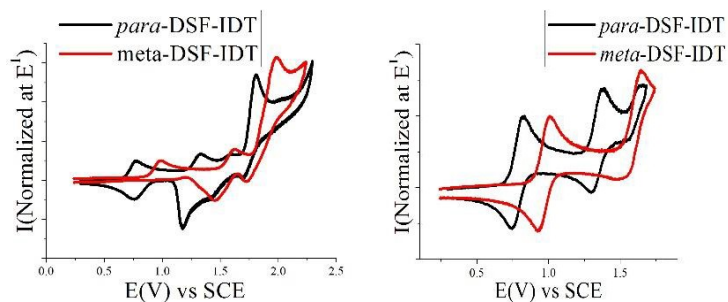


Figure 7. Cyclic voltammeteries (Bu_4NPF_6 0.2 M / CH_2Cl_2 , sweep-rate 100 mV s^{-1} , platinum disk working electrode, \varnothing 1 mm) in presence of *para*-DSF-IDT (in black) and *meta*-DSF-IDT (in red). Potential range: 0.25 to 2.25 V (Left) and 0.25 to 1.8 V (Right).

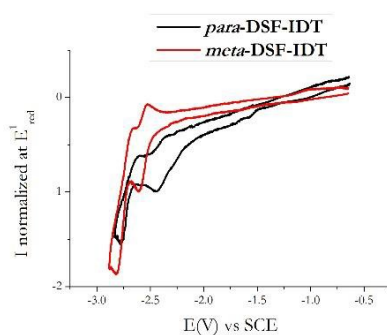


Figure 8. Cyclic voltammeteries (sweep-rate 100 mV s^{-1}) recorded in Bu_4NPF_6 0.1 M / DMF, in presence of *para*-DSF-IDT (in black) and *meta*-DSF-IDT (in red) (platinum disk working electrode, \varnothing 1mm).

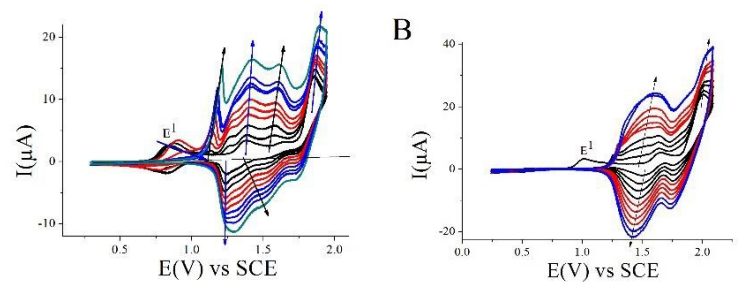


Figure 9. Cyclic voltammograms (Bu_4NPF_6 0.2 M / CH_2Cl_2 , sweep-rate 100 mV s^{-1} , platinum disk working electrode) in presence of **para-DSF-IDT** (Left) and **meta-DSF-IDT** (Right) in concentration $1.88 \cdot 10^{-3}$ M. Ten successive sweeps between 0.3 and 1.95 V (Left) or between 0.25 and 2.1 V (Right). The black arrows indicate the increase/decrease of the different waves along the 10 cycles.

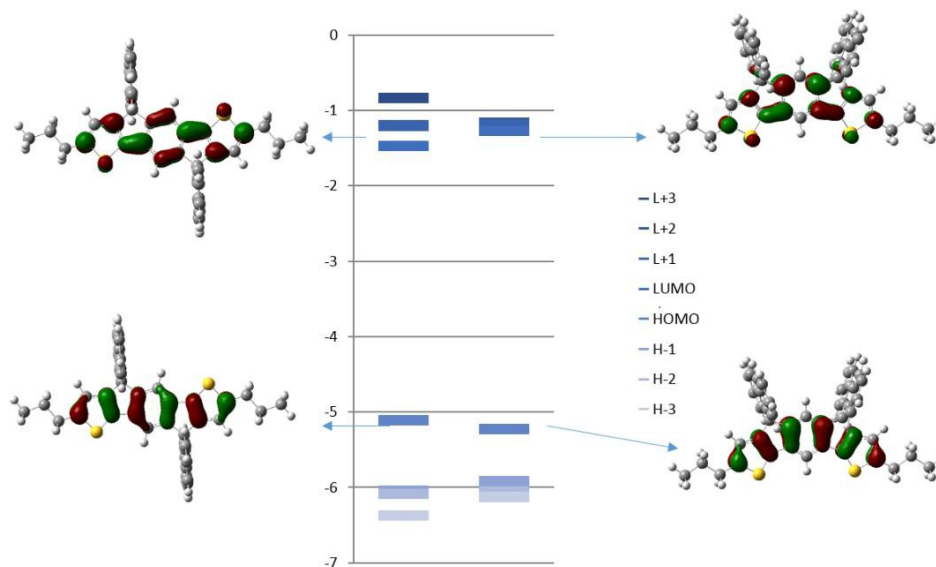


Figure 10. Calculated frontier molecular orbitals of **para-DSF-IDT** (left) and **meta-DSF-IDT** (right), after geometry optimization with DFT B3LYP/6-311G+(d,p) shown with a cut-off $0.04 [e \text{ bohr}^{-3}]^{1/2}$

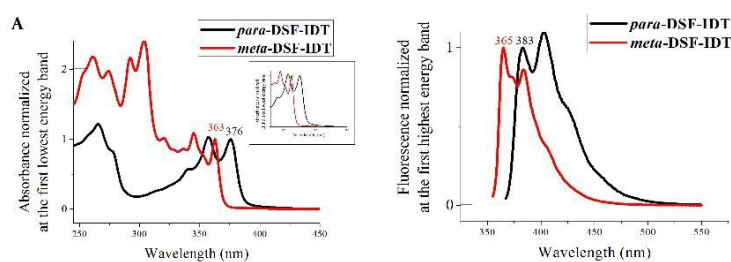


Figure 11. UV-Vis absorption spectra (Left) and emission spectra (Right) of **para-DSF-IDT** (black line) and **meta-DSF-IDT** (red line) in cyclohexane. $\lambda_{\text{exc}} = 358 \text{ nm}$ for **para-DSF-IDT** and 345 nm for **meta-DSF-IDT**

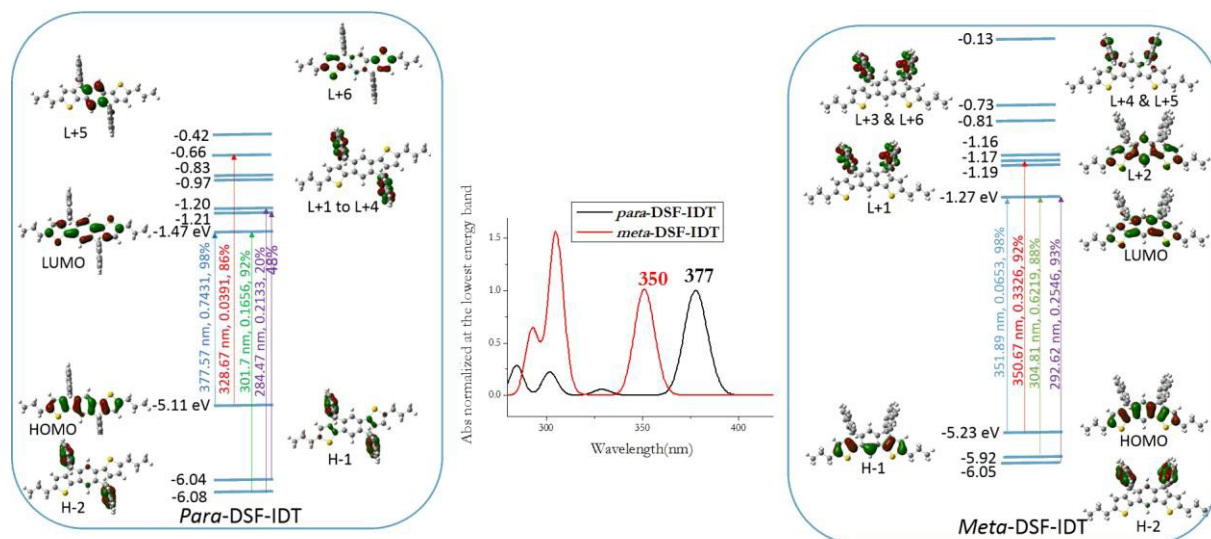


Figure 12. Theoretical UV spectra (inset) and representation of the energy levels and the main molecular orbitals involved in the electronic transitions of **para-DSF-IDT** (left) and **meta-DSF-IDT** (middle) obtained by TD-DFT B3LYP/6-311G+(d,p) shown with an isovalues of 0.04 [$e \text{ bohr}^{-3/2}$]

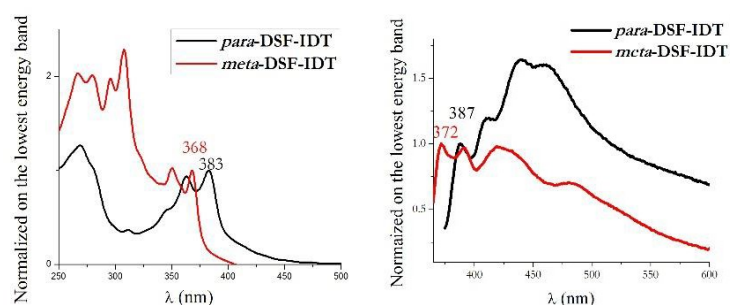


Figure 13. Normalized absorption (left) and emission spectra of spin-coated films (from THF at a concentration of 10mg/mL) of **meta-DSF-IDT** (red line, $\lambda_{\text{exc}}=362 \text{ nm}$) and **para-DSF-IDT** (black line, $\lambda_{\text{exc}}=352 \text{ nm}$)

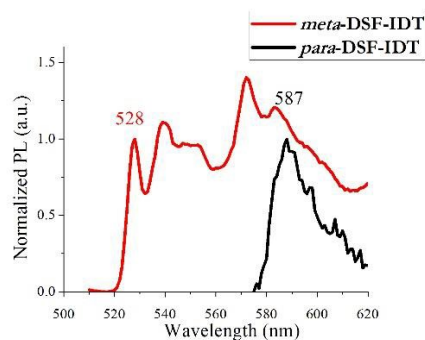
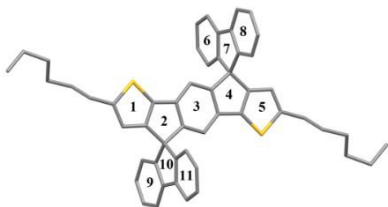
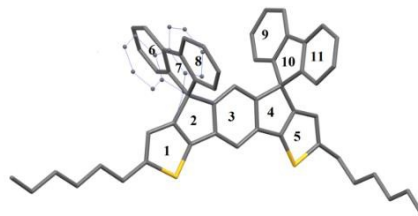


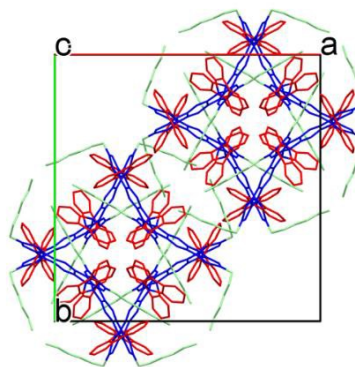
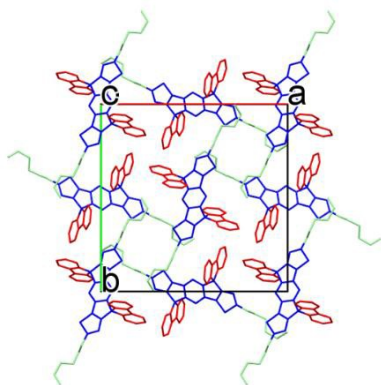
Figure 14. Emission spectra at 77K of **para-DSF-IDT** (black line) and **meta-DSF-IDT** (red line) in 2-Me-THF



***Para*-DSF-IDT**



***Meta*-DSF-IDT**



Catched eyes figure